Liquid Crystalline Behavior of Graphene Oxide in the Formation and Deformation of Tough Nanocomposite Hydrogels

ARTICLE *in* LANGMUIR · NOVEMBER 2014

Impact Factor: 4.46 · DOI: 10.1021/la503815y · Source: PubMed

Langmuir

Article

pubs.acs.org/Langmuir

Liquid Crystalline Behavior of Graphene Oxide in the Formation and Deformation of Tough Nanocomposite Hydrogels

Zhongcheng Zhu,[†] Guoshan Song,[†] Jiaqi Liu,[‡] Philip G. Whitten,*[,§] Luqi Liu,[∥] and Huiliang Wang*[,†]

[†]Beijing Key Laboratory of Energy Conversion and Storage Materials, College of Chemistry, Beijing Normal University, Beijing 100875, P. R. China

[‡]Department of Chemistry, Capital Normal University, Beijing 100048, P. R. China

[§]Intelligent Polymer Research Institute, ARC Centre of Excellence for Electromaterials Science, AIIM Facility, Innovation Campus, University of Wollongong, Wollongong, NSW 2522, Australia

[∥]National Center for Nanoscience and Technology, China, Beijing 100190, P. R. China

Supporting Information

ABSTRACT: In this paper, we report the formation and transformation of graphene oxide (GO) liquid crystalline (LC) structures in the synthesis and deformation of tough GO nanocomposite hydrogels. GO aqueous dispersions form a nematic LC phase, while the addition of poly(*N*-vinylpyrrolidone) (PVP) and acrylamide (AAm), which are capable of forming hydrogen bonding with GO nanosheets, shifts the isotropic/nematic transition to a lower volume fraction of GO and enhances the formation of nematic droplets. During the gelation process, a phase separation of the polymers and GO nanosheets is accompanied by the directional assembly of GO nanosheets, forming large LC tactoids with a radial GO configuration. The shape of the large tactoids evolves from a sphere to a toroid as the tactoids increase in size. Interestingly, during cyclic uniaxial tensile deformation a reversible LC transition is observed in the very tough hydrogels. The isolated birefringent domains and the LC domains in the tactoids in the gels are highly oriented under a high tensile strain.

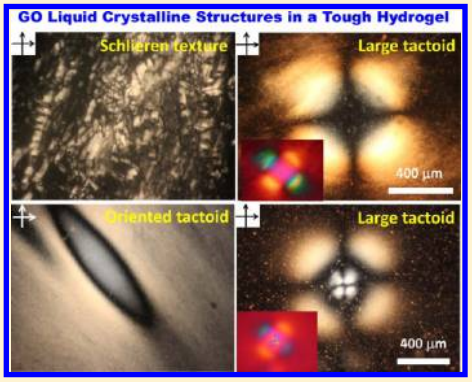

INTRODUCTION

Liquid crystal (LC) refers to a mesomorphic anisotropic state in which the constituents exhibit long-range directional order but no positional order. Many attempts have been made to introduce LC structures into hydrogels, and in some cases, macroscopically anisotropic hydrogels are formed, which mimic the microstructures and properties of biological tissues and hence might have potential applications in the fields of artificial muscles, membranes, and biomedical science.[1−3] The main strategies toward developing LC hydrogels include utilizing amphiphilic polymers or block copolymers, which are capable of forming LC domains as the building materials,[4−6] and introducing polymeric or more often inorganic nanoparticles exhibiting LC behavior, such as cellulose nanocrystals,[7] chitin rodlike particles,[8] and inorganic clay nanosheets[9,10] into hydrogel matrices.

Graphene, as the first example of a truly two-dimensional material consisting of a single atomic layer of graphite, has drawn immense attention in science and technology due to its excellent mechanical properties and superior thermal and electrical conductivities.[11−13] The liquid crystalline (LC) behavior of graphene and graphene oxide (GO) dispersions have been observed in recent years. Behabtu et al. first reported the LC behavior of a high concentration of graphene dispersed in chlorosulfonic acid.[14] GO is composed of a hydrophobic polyaromatic basal plane with a hydrophilic periphery, and it can function as a surfactant or amphiphile,[15−17] which facilitates the lyotropic LC behavior of GO in aqueous or organic solvent dispersions.[18−26] Yang et al. reported the LC behavior and property of GO dispersions under flow and revealed that the enhanced anisotropic and shear-thinning properties of GO solutions under flow condition are due to the self-assembled fiberlike and sheetlike structures at different concentrations.[21] Shen et al. demonstrated the macroscopic alignment of GO LC by applying low electric fields and pointed out the unique electro-optical property was due to the large Kerr coefficient for the first time.[18] It is well-known that the LC behavior of GO dispersions is strongly affected by both the pH value and ionic strength of impurities;[23] however, Zhao et al. reduced this effect by association of polyelectrolyte onto GO sheets and obtained a stable GO LC.[20]

The LC phase of graphene and GO dispersions facilitates the processing of neat graphitic macroscopic materials with extraordinary physical properties. For instance, Gao and co-workers were first to demonstrate the preparation of pure GO and reduced GO (RGO) fibers with high electrical conductivity

Received: September 24, 2014
Revised: November 15, 2014
Published: November 17, 2014

   dx.doi.org/10.1021/la503815y | *Langmuir* 2014, 30, 14648−14657

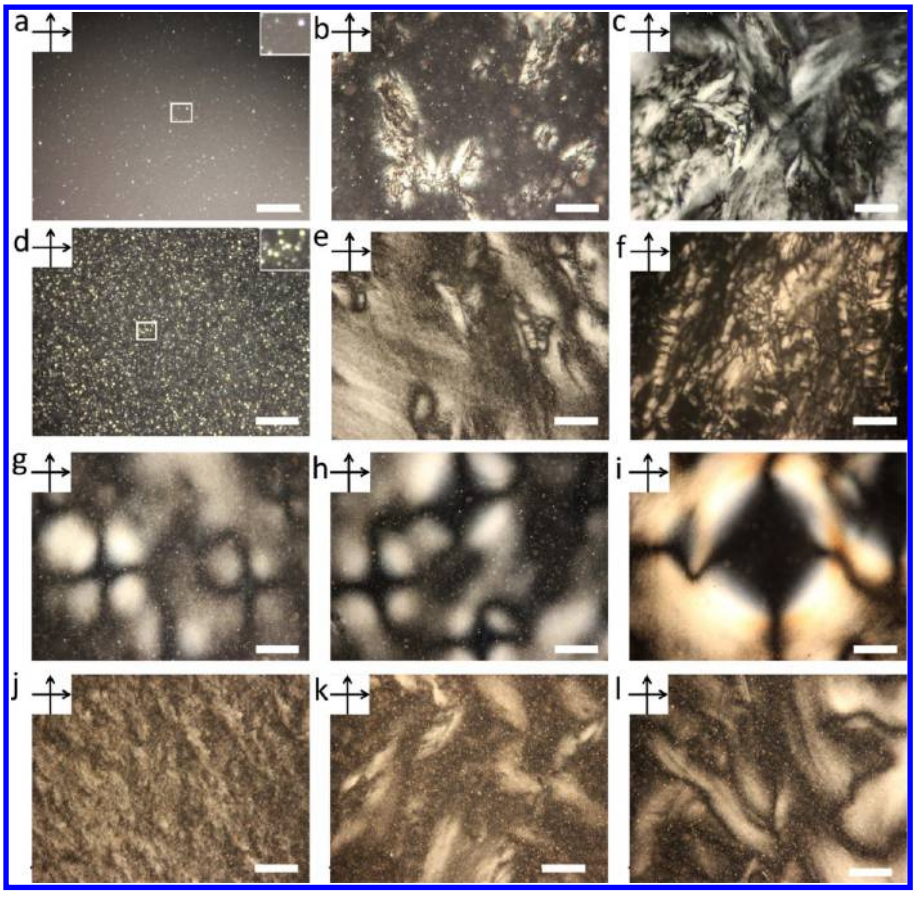

Figure 1. Crossed POM images of GO aqueous dispersions (a–c), GO/AAm/PVP aqueous dispersions (d–f), and GO/PAAm/PVP hydrogels (g–l) with different C_{GO}: (a, d, g) 2.5 mg/mL, (b, e, h) 5.0 mg/mL, and (c, f, i–l) 8.0 mg/mL. The insets in parts a and d show the magnified images of isolated birefringence domains. Scale bar: 200 μm. C_{AAm} = 6 mol/L and C_{PVP} = 0.04 g/mL.

and good mechanical performance through wet-spinning of GO and RGO dispersions[27] and recently GO LC fibers (or aerogels) with high tensile strength (0.5 GPa),[28] unconventional 100% knot efficiency,[29] and excellent supercapacitor performance.[30,31] Recently, polymer-grafted GO LC dispersions have also been used for developing nacre-mimetic material with excellent mechanical strength and toughness.[32,33]

Incorporating GO LC structures into hydrogels may reveal new and useful LC structures. Hydrogels with higher or anisotropic physical properties could feasibly result from gelation of an alignment of LC structures and hence expand their application. Many GO/polymer composites including hydrogels[34−39] with improved mechanical properties have been prepared. However, relatively little attention has been paid to the LC behavior of the GO nanocomposites. The only reported example was by Kim et al., who found that the LC structure of a GO dispersion can be maintained in a poly(acrylic acid) (PAA) matrix, and they also showed that hand-drawn fibers of PAA/water/GO exhibit strong birefringence with the GO platelets highly aligned along the mechanical drawing direction.[23] However, Kim et al. did not describe the transformation of the LC texture during deformation, and they did not note any changes to the LC structure upon the incorporation of PAA.

Recently, we reported the synthesis of very tough hydrogels physically cross-linked by the strong cooperative hydrogen bonding between pre-existing poly(*N*-vinylpyrrolidone) (PVP) and in situ polymerized polyacrylamide (PAAm).[40] In this work, we incorporate GO nanosheets into the tough hydrogels. The LC behavior of GO during the gelation process and in the gels under low and high strains is reported. The addition of poly(*N*-vinylpyrrolidone) (PVP) and acrylamide (AAm) promotes the formation of novel LC structures. Large toroid-shaped tactoids with a radial GO configuration are formed during the gelation process. Randomly distributed, isolated LC domains and the LC tactoids in the gels become highly oriented under an applied high tensile strain, and more interestingly, these transformations are reversible.

EXPERIMENTAL SECTION

Preparation of PAAm/PVP/GO Nanocomposite Hydrogels. The synthesis and characterizations of completely exfoliated GO sheets are provided in the Supporting Information. AAm/PVP/GO dispersions with fixed concentrations of the monomer AAm (ultra pure grade, Amresco Inc.) (C_{AAm} = 6.0 mol/L) and the pre-existing polymer PVP ($M_w = 4.0 \times 10^4$, Amresco Inc.) (C_{PVP} = 0.04 g/mL) and varying GO concentrations (C_{GO} = 0, 2.5, 5.0, and 8.0 mg/mL) were obtained by mixing AAm and PVP into the well-dispersed GO aqueous dispersions. The mixed dispersions were transferred into glass molds made by placing a silicone spacer with a thickness of 1 mm (or 2 and 4 mm) between two flat glass plates. Then the mixed dispersions were deaerated for about 15 min by bubbling with high-purity nitrogen at room temperature. It is necessary to mention that the gelation of the GO/AAm/PVP dispersions even occurred during the nitrogen-bubbling process. To ensure the full conversion of AAm and the formation of tough PAAm/PVP/GO composite hydrogels, the systems were kept at 50 °C for 36 h.

Polarized Optical Microscopy (POM) of LC Structures. Birefringence was observed with an optical microscope (OPTEC,

dx.doi.org/10.1021/la503815y | *Langmuir* 2014, 30, 14648−14657

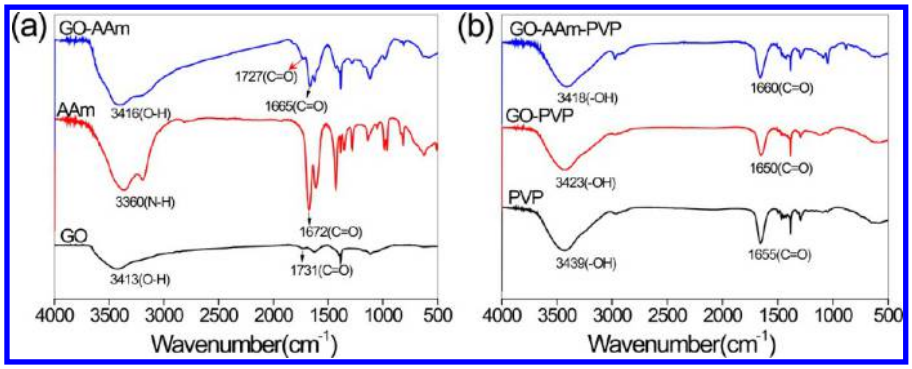

Figure 2. FT-IR spectra of (a) GO, AAm, and GO/AAm and (b) PVP, GO/PVP, and GO/AAm/PVP. $C_{GO} = C_{AAm} = C_{PVP} = 8$ mg/mL.

SMART-POL) equipped with a high-quality SLR camera (Canon, EOS600D) in transmission mode in a crossed polarized configuration, and a full-wave retardation plate was used to observe the orientation of GO LC structures. For the investigation of the formation and transformation of LC structures during the gel formation process, the GO/AAm/PVP dispersions in the glass molds were observed at room temperature, where the polymerization of AAm is assumed to be slower than at 50 °C.

To investigate the transformation of LC structures during the elongation of the hydrogels, the hydrogels were elongated to different maximum tensile strains, and then the two ends of the gel samples were fixed, and the large tactoids and other LC domains in the elongated samples were observed by crossed POM. The elongated samples were also rotated to different angles to observe the orientation of the LC structures.

FTIR Characterization. Fourier-transform infrared (FTIR) spectra of the dried GO sheets, AAm, and PVP and the dried GO/AAm, GO/PVP, and GO/AAm/PVP dispersions were recorded on a Nicolet-380 FT-IR spectrometer using the KBr method in the range of 400−4000 cm^{-1}.

SEM Observations. To investigate the microstructure of large tactoids, the hydrogel samples were swollen to 90 wt % water content and then plunged into liquid nitrogen for about 5 min. The frozen samples were subsequently freeze-dried until all the water was removed. The dried samples were cracked in the middle of the tactoids. After being sputter-coated with gold for 5 min, the morphologies of these fractured surfaces were observed with a Hitachi S-4800 cold field emission scanning electron microscope (Tokyo, Japan).

Tensile Mechanical Tests of GO Nanocomposite Gels. The dumbbell-shaped specimens for tensile tests were cut into standard size according to DIN-53504 S3 (overall length, 35 mm; width, 6 mm; inner width, 2 mm; gauge length, 10 mm; thickness, 1 mm), and they were coated with a thin layer of silicon oil to prevent the evaporation of water during the tests. The specimens were tested with an Instron 3366 electronic universal testing machine (Instron Corp.) at a crosshead speed of 800% mm min^{-1}. Stress and strain between $\varepsilon_t = 10$ and 30% were used to calculate initial elastic modulus (E). In order to obtain reliable values, at least three specimens per experimental point were tested in all mechanical tests. Cyclic measurements were performed in immediate succession with the same specimen at a maximum strain of 1000% eight times at a crosshead speed of 800% mm min^{-1}.

RESULTS AND DISCUSSION

LC Structures of GO/AAm/PVP Dispersions and Gels. The synthesis and chemical characterization of GO are provided in the Supporting Information (see Supporting Methods and Figure S1). The oxidized graphite flakes were completely exfoliated into single-layered GO sheets, with the individual GO sheets having a thickness in the range of 0.85−0.93 nm, as determined by both AFM (Supporting Information, Figure S2) and XRD (Supporting Information, Figure S3), which is consistent with the reported value.[41] The average lateral size of the GO sheets was measured to be 2.43 ± 1.33 μm by DLS and 3.6 ± 1.0 μm by SEM (Supporting Information, Figure S2). Note that the GO sheets produced here are slightly larger than or close to those reported by Kim et al.[23] and Xu et al.[25] By calculation, the GO sheets have an aspect ratio of more than 2600. Therefore, the critical GO concentration (C_{GO}) for LC formation (C^*) is about 1.6 mg/mL according to Onsager LC theory.[42]

The LC behavior of the GO aqueous dispersions with different GO concentrations (C_{GO}) was observed. Polarized optical microscopy (POM) images of the GO aqueous dispersions imaged between crossed polarizers are shown in Figure 1a−c. A nematic LC phase has formed as indicated by the distinct birefringent and/or Schlieren textures when viewed with POM.[43] Isolated birefringence domains are observed when C_{GO} is 2.5 mg/mL (Figure 1a), a value higher than C^*. The discrepancy between the theoretical and experimental C^* may be attributed to the flexible nature of the monolayered GO sheets and their polydispersity in size and thickness.[24] At the C_{GO} of 5.0 mg/mL, a combination of small isolated birefringence domains and large birefringent regions displaying vivid Schlieren texture appears (Figure 1b). Upon further increasing C_{GO} to 8.0 mg/mL, the whole dispersion displays Schlieren texture (Figure 1c). These results are consistent with previous reports.[23,25,26]

When the aqueous dispersions of GO are mixed with PVP and AAm, the resulting dispersions exhibit similar LC behavior as GO dispersions (Figure 1d−f). The main difference is that there are a greater number of isolated birefringence domains (Figure 1d) at the C_{GO} of 2.5 mg/mL and a greater volume fraction of Schlieren textures at higher C_{GO} (Figure 1e,f).

Determining the rheological property of dispersions is an alternative approach to characterizing LC formation. Previous rheological measurements showed that GO LC dispersions exhibit significant shear-thinning behavior.[21,44] Similarly, the GO dispersions in our work also show obvious shear-thinning behavior. In general, an LC emulsion (a dispersed LC phase in a solution) exhibits a relatively lower viscosity than a solution of the same concentration of reagents. The viscosity of GO dispersions is lowered by the addition of PVP and/or AAm, with the GO/AAm/PVP dispersion exhibiting the lowest relative viscosity (Supporting Information, Figure S4a). The POM and rheological results suggest that the presence of PVP and AAm shifts the isotropic/nematic transition to a lower volume fraction of GO and enhances the formation of nematic droplets.

dx.doi.org/10.1021/la503815y | Langmuir 2014, 30, 14648−14657

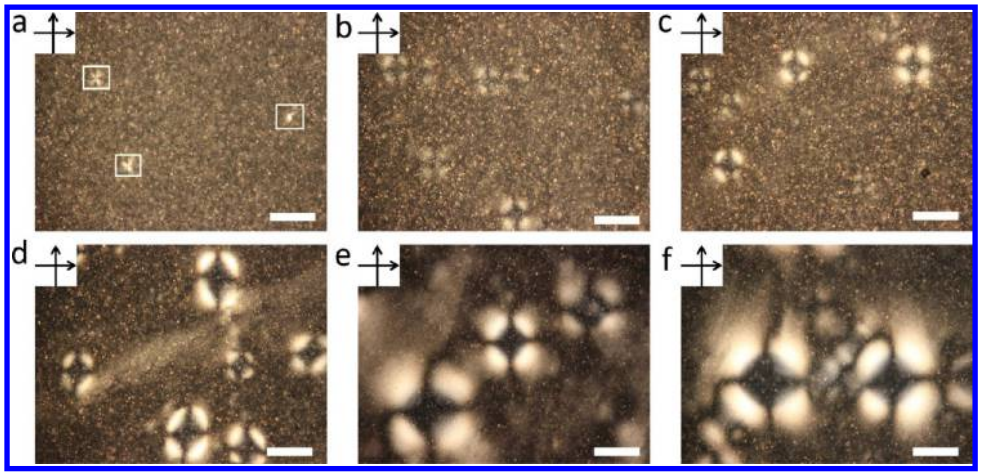

Figure 3. Crossed POM images in the formation of tactoids during the gelation of AAm/PVP/GO dispersion at room temperature for different times: (a) 0.5 h, (b) 1 h, (c) 2 h, (d) 4 h, (e) 8 h, and (f) 12 h. C_{GO} = 8.0 mg/mL. Scale bar: 500 μm.

FTIR characterization was conducted to understand the interactions between GO and PVP and/or AAm. There is a high density of oxygen-containing groups on the periphery of the GO sheets, and both PVP and AAm contain carbonyl and amino groups; therefore, hydrogen bonds (possibly cooperative hydrogen bonding) are formed between the GO sheets and the PVP and/or AAm molecules. The IR spectrum of GO contains the typical absorptions peaks attributed to the hydroxyl and carbonyl groups at 3413 and 1731 cm^{-1}, respectively (Figure 2a), while the IR spectrum of AAm shows the typical absorptions peaks attributed to the N−H and carbonyl groups at 3360 and 1672 cm^{-1}, respectively. When AAm is mixed with GO, the absorption peak attributed to the carbonyl group in GO shifts from 1731 to 1727 cm^{-1}, and the peak of the carbonyl group in AAm shifts from 1672 to 1665 cm^{-1}. In addition, the IR spectrum of PVP shows the typical absorption peaks attributed to the hydroxyl and carbonyl groups at 3439 and 1655 cm^{-1}, respectively (Figure 2b). While the mixture of PVP and GO (GO/PVP) exhibits absorption peaks from the same chemical groups at 3423 and 1650 cm^{-1}, respectively, both are shifted to lower wavenumbers. The observed shift in IR adsorption peaks upon adding GO to AAm and/or PVP can be explained by the hydrogen bonding between GO and AAm or PVP. Intermolecular hydrogen bonding is beneficial to stabilize the LC structures of binary mixtures.[45] Hence, neighboring GO sheets may be interconnected by PVP polymer chains via hydrogen bonding, facilitating the formation of larger LC structures.

The GO/AAm/PVP dispersions transform into hydrogels very easily, even at ambient temperature after the removal of dissolved oxygen (Supporting Information, Figure S4b). The XRD pattern of the dried GO/PAAm/PVP hydrogel shows a sharp diffraction peak at 2θ = 6.8°, corresponding to an interlayer spacing of 1.29 nm, while those for GO are 10.3° and 0.85 nm, respectively (Supporting Information, Figure S3), suggesting that polymer chains have intercalated into the interlayer of GO sheets. Unfortunately, it is not possible to obtain the interlayer spacing of GO nanosheets in the dispersions or hydrogels as the distance between GO sheets is too large for the XRD technique. As expected, the PAAm/PVP hydrogel without GO does not show LC structures (Supporting Information, Figure S5). The GO/PAAm/PVP hydrogels synthesized with different C_{GO} show LC structures that are substantially different from those of the GO dispersions and the AAm/PVP/GO dispersions, as the nitrogen bubbling of the dispersions and the polymerization process induce the change of the LC structures. The samples exhibiting large tactoids (also termed as LC droplets) that are heterogeneous also contain regions where isolated birefringence domains and large Schlieren textures dominate (Figure 1j−l). The large tactoids are found in all hydrogels, even when C_{GO} is only 2.5 mg/mL. The diameter of the tactoids increases with increasing C_{GO} (Figure 1g−i), and the average diameter of the tactoids at C_{GO} of 2.5 and 8.0 mg/mL are about 0.4 and 1.4 mm, respectively.

Formation and Transformation of Large Tactoids. To understand the formation and transformation of tactoids, we observed the gelation process of the GO/AAm/PVP dispersions at room temperature. In the very initial stage of gelation, some tactoids are formed. They are bigger than the isolated birefringent domains and exhibit different shapes under polarized light (Figure 3a). The relatively large tactoid in the middle right side of Figure 3a shows a bright central region and less bright outer region, and the other two relatively large tactoids exhibit four alternating white and dark regions meeting at the center, with the one shown in the upper left having more obvious white and dark regions. As the AAm polymerization time increases from 0.5 to 1 h, a greater number of large tactoids are formed (Figure 3b,c). Some of them have a crossed dark central region and four brighter leaves in the periphery, and the others have only two or three obvious leaves. From 2 h onward the large tactoids exhibit a regular shape with a crossed dark central region and four very bright leaves (Figure 3d−f). The increase of the tactoid diameter is investigated in more detail by observing the growth of an identical tactoid (Supporting Information, Figure S6). The diameter of the tactoid increases almost linearly with time until 12 h and then remains almost constant (Figure 4). Note that where there is a massive decrease in the growth rate of the tactoid, the LC tactoid diameter coincides with the thickness of the hydrogel (1 mm).

It is well-known that the director field configurations of tactoids vary as a function of their size.[46] From the observation of the nucleation and transformation of the tactoids, it is possible to know the change of their director field configurations. Figure 5 shows the nucleation and transformation of the tactoids and their director field configurations. The crossed POM image of a small tactoid formed at a

dx.doi.org/10.1021/la503815y | *Langmuir* 2014, 30, 14648−14657

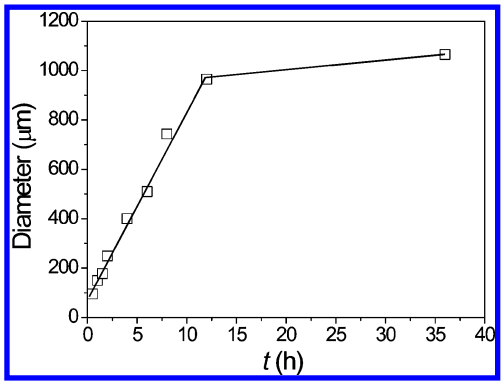

Figure 4. Change of the diameter of an identical tactoid during the gelation of the AAm/PVP/GO dispersion (C_{GO} = 8.0 mg/mL) for different times.

polymerization time of less than 10 min shows a single bright region (Figure 5a1), indicating that it has a uniform configuration (Figure 5a3). The tactoid (100 μm) observed at 0.5 h exhibits eight alternating white and dark regions meeting at the center under crossed polarized light (Figure 5b1). The slightly bigger tactoids observed at a polymerization time of 1 h show a dark central region and two bigger and brighter as well as two smaller and less bright leaves, due to the uneven distribution of GO sheets [Figures 5c1 and S7 (Supporting Information)].

When the gels containing large tactoids (polymerization times ≥2 h) were rotated under crossed polarized light, the location of dark and bright regions of the tactoid did not change obviously with the rotation angle (Supporting Information, Figure S8a and Movie S1), indicating that the LC domain has a radial configuration. Crossed polarization light microscopy with a retardation plate was used to determine whether the director of the LC domains is parallel or perpendicular to the tangent of the circle defining the tactoid. It is known that if the nematic director is perpendicular to the retardation plate, then the tactoid will appear orange, whereas in the parallel orientation it will appear blue. The small tactoid shows only yellow color (Figure 5a2), indicating that the GO sheets in it are aligned perpendicular to the nematic director. For the tactoids with a radial configuration, they show both orange and blue colors in the direction axes perpendicular and parallel to the retardation plate, respectively, indicating that the

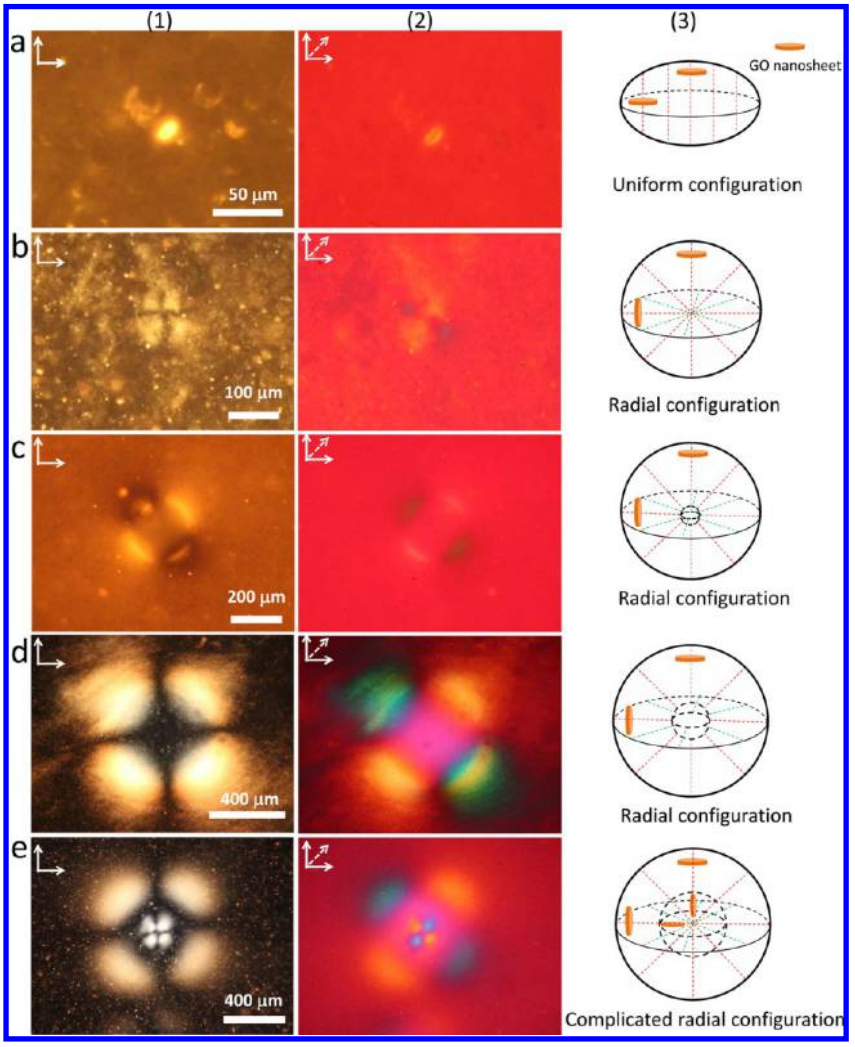

Figure 5. Formation and transformation of tactoids during different stages of gelation in a 2 mm thick hydrogel film. (a) In the very initial stage (<10 min) and after (b) 0.5 h, (c) 1 h, and (d and e) 12 h. Typical crossed POM images of tactoids without (1) and with (2) a retardation plate and their simulated LC configurations (3). The LC field directors in both horizontal and vertical directions are shown as dashed lines, which are perpendicular to the orientation of GO nanosheets. C_{AAm} = 6 mol/L, C_{PVP} = 0.04 g/mL, and C_{GO} = 8.0 mg/mL.

dx.doi.org/10.1021/la503815y | *Langmuir* 2014, 30, 14648−14657

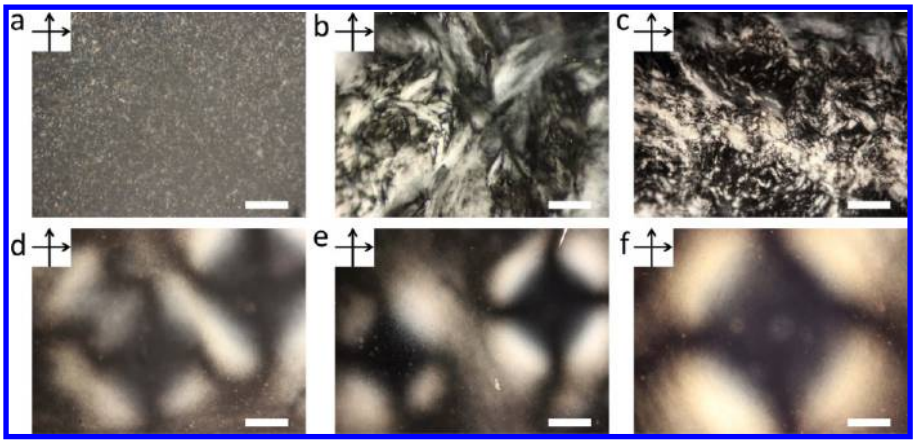

Figure 6. Crossed POM images of a GO dispersion (a–c) and a GO nanocomposite hydrogel (d–f) in aqueous solutions with different pH values: (a, d) pH 1.0, (b, e) pH 7.0, and (c, f) pH 12.0. C_{GO} = 8 mg/mL. Scale bar: (a–c) 200 μm and (d–f) 500 μm.

GO sheets in them are aligned perpendicular to the nematic director. Hence, it was determined that the planes of the GO nanosheets are aligned tangentially to the circle tactoid cross-section, as proposed by Higgins and co-workers.[47,48] Hurt and co-workers also observed similar alignment of GO nanosheets around the trapped air bubbles during the drying of GO suspensions.[26]

For the tactoids observed for a polymerization time ≥1 h, a large dark central region is observed without the bright leaves approaching a central extinction point. The large dark central region corresponds to a circular bright region under parallel polarized light and transmitted light without an analyzer and a polarizer (Supporting Information, Figure S9a) and to a large pore surrounded by many smaller pores when freeze-dried tactoids are viewed with SEM (Supporting Information, Figure S9b1). It is necessary to mention that the large pore in the sample for SEM investigation (Supporting Information, Figure S9b1) is formed in the freeze-drying process of highly swollen hydrogels (95 wt % water content) due to the collapse of polymers that are very possibly less cross-linked, as there are no observable pores or air bubbles in the as-prepared samples and the central region of the tactoids is full of amorphous polymeric hydrogel (Supporting Information, Figure S10). The microscopy of the dark central region is consistent with an unusual toroidal shape tactoid (Figure 5d1) that has an amorphous central region (Figure 5d3).

Since the size of the tactoids are comparable to or even larger than the gel film thickness of 1 mm, the growth of tactoids may be restrained and hence alter their director field configurations. To explore the effect of overall sample confinement on final tactoid diameter, hydrogels with a thickness of 2 and 4 mm were prepared. Larger diameter tactoids were obtained, and some of them exhibit more complicated and interesting shapes under polarized light. Except for the alternating white and dark regions in the outer part, alternating white and dark regions meeting at the center are also found in the dark central region (Figure 5e1). SEM imaging of freeze-dried specimens shows that there are some materials radially distributed in the center of the large pore (Supporting Information, Figure S9b2). The appearance of yellow and blue colors in the central region of the retardation plate is exactly opposite to that in the outer region (Figure 5e2), suggesting that the GO sheets in the central region are aligned parallel to the nematic director (Figure 5e3). When the gel was rotated, the orientation of dark and bright regions in the central or outer part of the tactoid does not change obviously with the rotation angle (Supporting Information, Figure S8b and Movie S2). Therefore, the tactoids formed in a thicker gel have a complicated radial configuration incorporating another radial configuration in the center (Figure 5e3).

These observations might provide a preliminary understanding of the mechanism of the formation and transformation of the tactoids. Polymerization-induced phase separation is often observed in monomer/LC dispersions and in polymer monomer solutions.[49−53] In our work, the formation of large tactoids in the GO nanocomposite hydrogels, illustrating that the system is not thermodynamically stable, could also be driven by the phase separation induced by the exothermic polymerization process. The polymerization of AAm leads to the formation of polymer-rich and polymer-poor domains in the GO LC dispersions. As part of the AAm molecules is hydrogen-bonded to GO nanosheets and PVP chains, the polymerization of AAm also leads to the increase in the local concentration of GO nanosheets and the formation of tactoids. In the early stage of polymerization, the conversion of AAm is low, and hence, only small tactoids are formed. The smallest tactoids have a uniform director field configuration without defect (Figure 5a), and the larger tactoids have a radial configuration with a point defect in the center (Figure 5b). They are consistent with the theoretical and experimental results on tactoids of discotic particles, whose configurations transit from a radial to a uniform director field upon decreasing tactoid size.[46] With the progress of gelation, more monomer molecules are polymerized and more physical cross-links are formed in the system; the cross-links hold the small tactoids together to form larger tactoids.[50] They have a radial configuration with a toroid shape and a larger defect in the center (Figure 5d), possibly due to phase separation gradually growing from the point defect in the center, forming a central region with mainly less cross-linked polymers and an outer region with highly cross-linked polymers and GO nanosheets. It is necessary to mention that the phase separation is not complete, as there are some GO nanosheets left in the central region. After the polymerization, the tactoids in the GO nanocomposite hydrogels are very stable. The phase separation process also leads to the orientation of GO nanosheets, which are perpendicular to the field director in the outer region of the tactoids. The possible reason for the formation of the complicated radial configuration incorporating another radial configuration in the center (Figure 5e) is that the GO

dx.doi.org/10.1021/la503815y | *Langmuir* 2014, 30, 14648−14657

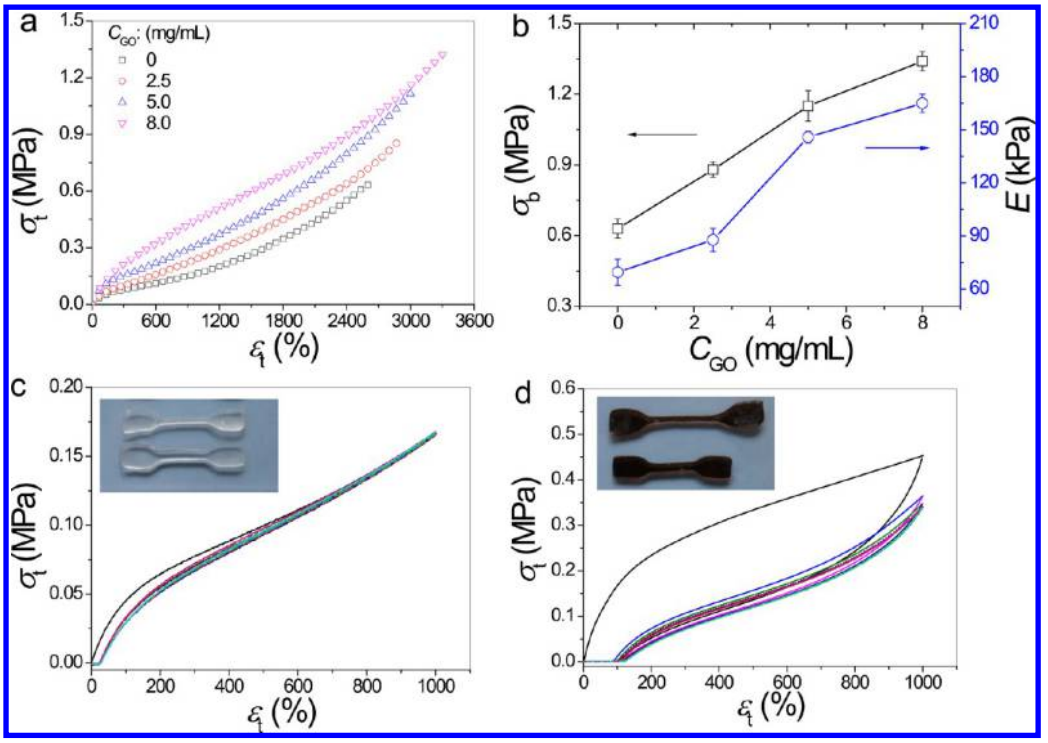

Figure 7. Tensile mechanical properties of GO nanocomposite hydrogels. Tensile stress–strain (σ_t–ε_t) curves (a) and tensile strength (σ_t) and elastic modulus (E) (b) of the hydrogels with different C_{GO}. Cyclic loading–unloading curves of the hydrogels without (c) and with (d) C_{GO} of 8.0 mg/mL to the maximum strain of 1000% for eight cycles. The insets in parts c and d are photographs of hydrogel specimens after cyclic tensile tests with comparison to the original specimens. Reaction conditions: C_{AAm} = 6 mol/L and C_{PVP} = 0.04 g/mL. The water content of the gels was about 69.1%.

nanosheets embedded in them cannot be totally expelled from the central region (Supporting Information, Figure S9b2), and the left GO nanosheets are aligned parallel to the field director due to the shear force induced by the expansion of the central dark (polymer) region.

The pH Stability of the Large Tactoids. The LC behavior of GO dispersions is strongly affected by the pH values of their environment.[23] Our experiments also show that lowering pH induces the destruction of Schlieren textures into small isolated birefringence domains, whereas the increase of pH leads to an increase in the volume fraction of Schlieren textures (Figure 6a–c). In contrast, the LC phase in the hydrogel samples does not change with pH value, as evidenced by the very similar tactoids in the gels swelled in water with different pH values (Figure 6d–f), with larger tactoids in an alkaline solution (pH 12.0) than in acidic (pH 1.0) and neutral environments (pH 7.0). The diameters of the respective tactoids are consistent with the swelling ratios of the gels (Supporting Information, Figure S11). These results suggest that the pH instability of the GO LC phase can be overcome by incorporating it into a tough hydrogel, as the robust gel network restrains the movements of GO nanosheets.

Mechanical Properties of the GO Nanocomposite Hydrogels. The GO nanocomposite hydrogels exhibit excellent mechanical properties. Figure 7a shows the typical stress–strain (σ_t–ε_t) curves of the gels synthesized with different C_{GO}. In comparison to the PAAm/PVP hydrogel without GO, the GO nanocomposite hydrogels exhibit higher tensile strength (σ_b), elongation at break (ε_b), and initial elastic modulus (E). The GO nanocomposite gels show very high elongation at break, generally more than 2800%, and the highest is about 3300%. The σ_b, ε_b, and E of the gels all increase with increasing C_{GO} (Figure 7a,b). The GO nanocomposite hydrogel synthesized with a C_{GO} of 8.0 mg/mL has a very high ε_b of 1.34 MPa, which is 2 times that of the hydrogel without GO. Similarly, the E of the GO nanocomposite hydrogels increases from 70 to 165 kPa with an increase of C_{GO} from 0 to 8.0 mg/mL. The tensile mechanical properties of the GO nanocomposite hydrogels are among the best of the toughest hydrogels ever reported.[54−57] The results indicate that the incorporation of GO nanosheets into a tough gel can further improve its mechanical properties to achieve a very tough GO nanocomposite hydrogel.

Cyclic tensile tests were performed to reveal the energy dissipation and deformation recoverability of the gels. The loading–unloading curves of the gels cyclically stretched to a maximum strain of 1000% eight times are shown in Figure 7c,d. The hydrogel without GO shows a very high resilience (resilience is identified as the area under the recovery curve divided by the area under the loading curve) of more than 0.90 in the first cycle and up to 0.97 in the following cycles [Figures 7c and S12 (Supporting Information)]. For the GO nanocomposite hydrogels, relatively low resilience is observed in the first and the following cycles. The resilience of the GO composite hydrogels decreases with an increase of C_{GO}, and it is about 0.88 after eight cycles for the GO nanocomposite hydrogel with a C_{GO} of 8.0 mg/mL [Figures 7d and S12 (Supporting Information)]. The observation of a lower resilience and a higher residual strain in the GO nanocomposite hydrogel with a higher C_{GO} is consistent with nanocomposite gels formed with platelike colloids.[58]

The E and ε_b of the gels increase with increasing GO concentration, due to the increasing cross-linking density induced by the hydrogen bonding between the GO nanosheets

dx.doi.org/10.1021/la503815y | Langmuir 2014, 30, 14648−14657

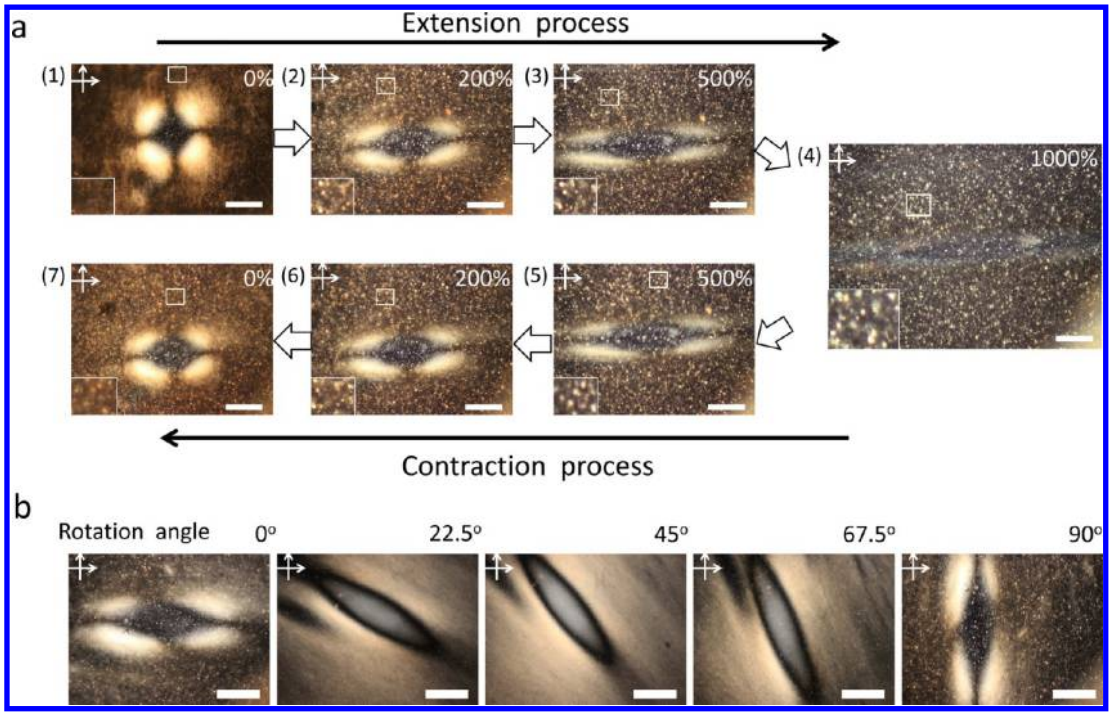

Figure 8. (a) Crossed POM images of a large tactoid in the hydrogel during cyclic tensile deformation: (1−4) the extension process with the strain increasing from 0% to 1000% and (4−7) the contraction process with the strain decreasing from 1000% to 100%. The insets in lower left corner in part a are the enlarged POM images in the elongated gel under different tensile strains. (b) Crossed POM images of the tactoid in the gel sample elongated to 300% strain and then rotated to various angles. Scale bar: 500 μm.

and the PVP and PAAm chains. Usually, an increase in E and σ_b leads to a decrease in ε_b. However, a significant increase of ε_b with increasing GO concentration is also observed in the GO nanocomposite hydrogels. Possible reasons include that buckled GO nanosheets are easy to be straightened, the hydrogen bonding between GO nanosheets and polymer chains is transient under an applied force that dissipates energy, the GO nanosheets are relatively large multifunctional cross-link sites, and tactoids may blunten crack tips. The straightening of buckled GO nanosheets and the breakage of hydrogen bonding cannot be totally recovered, leading to the lower resilience of the GO nanocomposite hydrogels [Figures 7c,d and S12 (Supporting Information)] and the incomplete recovery of LC tactoids (Figure 8a).

Transformation of LC Structure in the Deformation of Gels. The high tensile strength, high elongation, and the good shape recoverability of the gels allowed study of the transition of LC structure within hydrogels from low to high strains. POM images were taken on a GO nanocomposite hydrogel specimens at different strains in a loading−unloading process.

We first examined the transformation of the large tactoids in the gels during cyclic tensile deformation. The tactoid undergoes a shape deformation along the elongation direction (Figure 8a). The four bright regions in the periphery are elongated by an increase of tensile strain, and they almost disappear at the strain of 1000%. Furthermore, it can be found that both a greater number and an increased birefringent intensity of isolated birefringence domains appear, even in the central part of the tactoid, upon increase of tensile strain. In the contraction process, the tactoid appears again and gradually recovers its original shape as the tensile strain decreases from 1000% to 100% (Figure 8a). The tactoid cannot completely recover its original shape, as there is residual strain (Figure 7d). In addition, the number and brightness of the isolated birefringence domains also decrease. Similar increase and decrease of isolated birefringence domains in other parts of the gel were also observed during the extension and retraction of the gel (Supporting Information, Figure S13a). These results suggest that the deformation of the LC structures under high strain is reversible.

The elongated gel sample was rotated to different angles on the sample stage and was observed under the crossed polarized light. At the rotation angles other than 0° and 90°, the four bright regions of the tactoid disappear; instead, the tactoid (even the central part of it) and the isolated birefringence domains all become bright, and the highest birefringence is observed at 45° [Figure 8b and Movie S3 (Supporting Information)]. Highly oriented LC structures can be found in the bright regions. A similar orientation of isolated birefringence domains in other parts of the elongated gel is also observed (Supporting Information, Figure S13b). Kim et al. reported that in the dried gels the GO platelets can be highly oriented under drawing.[23] Our work proves that in the uniaxially stretched swollen gels the LC domains are also highly oriented along the elongation direction.

The reasons for the transformation and orientation of LC structures are similar to those discussed for the mechanical properties. The breakage of hydrogen bonding between GO nanosheets and polymer chains under an applied force leads to the transformation of large tactoids into isolated birefringence domains; meanwhile, the rotation of flexible GO nanosheets along the elongation direction leads to their orientation and brighter birefringence. When the applied force is released, the entropy associated with stretching a polymer chain is decreased as the polymer chains take a more random configuration and the GO sheets return to their original configuration, leading to the recovery of large tactoids and the random orientation distribution of isolated birefringence domains.

dx.doi.org/10.1021/la503815y | *Langmuir* 2014, 30, 14648−14657

CONCLUSIONS

In summary, we observed the formation and transformation of LC structures in the formation and deformation of a tough hydrogen-bonded GO nanocomposite hydrogel. The GO aqueous dispersions containing a monomer (AAm) and especially a polymer (PVP), which is capable of forming hydrogen bonding with GO, can form more isolated birefringence domains and Schlieren textures. We believe that some other small molecular weight molecules and polymers might also facilitate the formation of LC structures of GO. Further study on the hydrogen-bonding interactions between GO and the small molecular weight molecules or polymers and their effect on the LC behavior of GO has important scientific significance and may lead to the development of novel LC materials. During the gelation process, the phase separation induced by the polymerization of the monomer molecules and the increase of cross-linking density between GO and the polymer chains leads to the formation of tactoids that undergo several configuration transformations. The finally obtained large tactoids have a toroid shape where the GO sheets have a radial configuration or a complicated radial configuration. To the authors' knowledge, the complicated radial configuration incorporating another radial configuration in the center is observed for the first time. The GO nanocomposite hydrogels synthesized in this work have excellent mechanical properties, which are among the best ever reported. Therefore, the transition of the LC structures in the mechanical deformation of the hydrogels can be studied even to very high strains. We observed the reversible transition of GO LC structures during cyclic tensile tests for the first time. The LC structures can be highly oriented along the elongation direction. The orientated LC structures are likely to be maintained by some methods, such as drying the samples under a strain. The tough GO nanocomposite hydrogels with reversible LC transition and highly oriented LC structures may find some potential applications in optical materials and other fields.

ASSOCIATED CONTENT

Supporting Information

Supporting methods, Figures S1−S13, and Movies S1−S3. This material is available free of charge via the Internet at http://pubs.acs.org.

AUTHOR INFORMATION

Corresponding Authors

*P.G.W. e-mail: whitten@uow.edu.au.

*Requests for materials should be addressed to H.W. (e-mail: wanghl@bnu.edu.cn).

Notes

The authors declare no competing financial interest.

ACKNOWLEDGMENTS

The authors appreciate financial support from the National Science Foundation of China (No. 21274013), the Fundamental Research Funds for the Central Universities.

REFERENCES

(1) Wu, Z. L.; Sawada, D.; Kurokawa, T.; Kakugo, A.; Yang, W.; Furukawa, H.; Gong, J. P. Strain-induced molecular reorientation and birefringence reversion of a robust, anisotropic double-network hydrogel. *Macromolecules* **2011**, *44*, 3542−3547.

(2) Haque, M. A.; Kurokawa, T.; Gong, J. P. Anisotropic hydrogel based on bilayers: Color, strength, toughness, and fatigue resistance. *Soft Matter* **2012**, *8*, 8008−8016.

(3) Weiss, F.; Finkelmann, H. Hexagonal lyotropic liquid crystalline hydrogels: Influence of uniaxial stress and pH value on the anisotropic swelling behavior. *Macromolecules* **2004**, *37*, 6587−6595.

(4) Kaneko, T.; Nagasawa, H.; Gong, J. P.; Osada, Y. Liquid crystalline hydrogels: Mesomorphic behavior of amphiphilic polyacrylates bearing cholesterol mesogen. *Macromolecules* **2004**, *37*, 187−191.

(5) Wu, Z. L.; Furukawa, H.; Yang, W.; Gong, J. P. Mesoscopic network structure of a semi-rigid polyion complex nested in a polycationic hydrogel. *Adv. Mater.* **2009**, *21*, 4696−4700.

(6) Becht, G. A.; Sofos, M.; Seifert, S.; Firestone, M. A. Formation of a liquid-crystalline interpenetrating poly(ionic liquid) network hydrogel. *Macromolecules* **2011**, *44*, 1421−1428.

(7) Kelly, J. A.; Shukaliak, A. M.; Cheung, C. C. Y.; Shopsowitz, K. E.; Hamad, W. Y.; MacLachlan, M. J. Responsive photonic hydrogels based on nanocrystalline cellulose. *Angew. Chem., Int. Ed.* **2013**, *52*, 8912−8916.

(8) Belamie, E.; Davidson, P.; Giraud-Guille, M. M. Structure and chirality of the nematic phase in alpha-chitin suspensions. *J. Chem. Phys. B* **2004**, *108*, 14991−15000.

(9) Paineau, E.; Dozov, I.; Bihannic, I.; Baravian, C.; Krapf, M.-E. M.; Philippe, A.-M.; Rouziere, S.; Michot, L. J.; Davidson, P. Tailoring highly oriented and micropatterned clay/polymer nanocomposites by applying an ac electric field. *ACS Appl. Mater. Interfaces* **2012**, *4*, 4296−4301.

(10) Miyamoto, N.; Shintate, M.; Ikeda, S.; Hoshida, Y.; Yamauchi, Y.; Motokawa, R.; Annaka, M. Liquid crystalline inorganic nanosheets for facile synthesis of polymer hydrogels with anisotropies in structure, optical property, swelling/deswelling, and ion transport/fixation. *Chem. Commun.* **2013**, *49*, 1082−1084.

(11) Lee, C.; Wei, X.; Kysar, J. W.; Hone, J. Measurement of the elastic properties and intrinsic strength of monolayer graphene. *Science* **2008**, *321*, 385−388.

(12) Balandin, A. A.; Ghosh, S.; Bao, W.; Calizo, I.; Teweldebrhan, D.; Miao, F.; Lau, C. N. Superior thermal conductivity of single-layer graphene. *Nano Lett.* **2008**, *8*, 902−907.

(13) Rao, C. N. R.; Sood, A. K.; Subrahmanyam, K. S.; Govindaraj, A. Graphene: The new two-dimensional nanomaterial. *Angew. Chem., Int. Ed.* **2009**, *48*, 7752−7777.

(14) Behabtu, N.; Lomeda, J. R.; Green, M. J.; Higginbotham, A. L.; Sinitskii, A.; Kosynkin, D. V.; Tsentalovich, D.; Parra-Vasquez, A. N. G.; Schmidt, J.; Kesselman, E.; Cohen, Y.; Talmon, Y.; Tour, J. M.; Pasquali, M. Spontaneous high-concentration dispersions and liquid crystals of graphene. *Nat. Nanotechnol.* **2010**, *5*, 406−411.

(15) Kim, J.; Cote, L. J.; Huang, J. Two dimensional soft material: New faces of graphene oxide. *Acc. Chem. Res.* **2012**, *45*, 1356−1364.

(16) Kim, J.; Cote, L. J.; Kim, F.; Yuan, W.; Shull, K. R.; Huang, J. Graphene oxide sheets at interfaces. *J. Am. Chem. Soc.* **2010**, *132*, 8180−8186.

(17) Cote, L. J.; Kim, J.; Tung, V. C.; Luo, J.; Kim, F.; Huang, J. Graphene oxide as surfactant sheets. *Pure Appl. Chem.* **2011**, *83*, 95−110.

(18) Shen, T.-Z.; Hong, S.-H.; Song, J.-K. Electro-optical switching of graphene oxide liquid crystals with an extremely large Kerr coefficient. *Nat. Mater.* **2014**, *13*, 394−399.

(19) Dan, B.; Behabtu, N.; Martinez, A.; Evans, J. S.; Kosynkin, D. V.; Tour, J. M.; Pasquali, M.; Smalyukh, I. I. Liquid crystals of aqueous, giant graphene oxide flakes. *Soft Matter* **2011**, *7*, 11154−11159.

(20) Zhao, X.; Xu, Z.; Xie, Y.; Zheng, B.; Kou, L.; Gao, C. Polyelectrolyte-stabilized graphene oxide liquid crystals against salt, pH, and serum. *Langmuir* **2014**, *30*, 3715−3722.

(21) Yang, X.; Guo, C.; Ji, L.; Li, Y.; Tu, Y. Liquid crystalline and shear-induced properties of an aqueous solution of graphene oxide sheets. *Langmuir* **2013**, *29*, 8103−8107.

(22) Gudarzi, M. M.; Moghadam, M. H. M.; Sharif, F. Spontaneous exfoliation of graphite oxide in polar aprotic solvents as the route to

produce graphene oxide−organic solvents liquid crystals. *Carbon* **2013**, *64*, 403−415.
(23) Kim, J. E.; Han, T. H.; Lee, S. H.; Kim, J. Y.; Ahn, C. W.; Yun, J. M.; Kim, S. O. Graphene oxide liquid crystals. *Angew. Chem., Int. Ed.* **2011**, *50*, 3043−3047.
(24) Aboutalebi, S. H.; Gudarzi, M. M.; Zheng, Q. B.; Kim, J.-K. Spontaneous formation of liquid crystals in ultralarge graphene oxide dispersions. *Adv. Funct. Mater.* **2011**, *21*, 2978−2988.
(25) Xu, Z.; Gao, C. Aqueous liquid crystals of graphene oxide. *ACS Nano* **2011**, *5*, 2908−2915.
(26) Guo, F.; Kim, F.; Han, T. H.; Shenoy, V. B.; Huang, J.; Hurt, R. H. Hydration-responsive folding and unfolding in graphene oxide liquid crystal phases. *ACS Nano* **2011**, *5*, 8019−8025.
(27) Xu, Z.; Gao, C. Graphene chiral liquid crystals and macroscopic assembled fibres. *Nat. Commun.* **2011**, *2*, 571.
(28) Xu, Z.; Sun, H.; Zhao, X.; Gao, C. Ultrastrong fibers assembled from giant graphene oxide sheets. *Adv. Mater.* **2013**, *25*, 188−193.
(29) Xiang, C.; Young, C. C.; Wang, X.; Yan, Z.; Hwang, C.-C.; Cerioti, G.; Lin, J.; Kono, J.; Pasquali, M.; Tour, J. M. Large flake graphene oxide fibers with unconventional 100% knot efficiency and highly aligned small flake graphene oxide fibers. *Adv. Mater.* **2013**, *25*, 4592−4597.
(30) Aboutalebi, S. H.; Jalili, R.; Esrafilzadeh, D.; Salari, M.; Gholamvand, Z.; Aminorroaya Yamini, S.; Konstantinov, K.; Shepherd, R. L.; Chen, J.; Moulton, S. E.; Innis, P. C.; Minett, A. I.; Razal, J. M.; Wallace, G. G. High-performance multifunctional graphene yarns: Toward wearable all-carbon energy storage textiles. *ACS Nano* **2014**, *8*, 2456−2466.
(31) Xu, Z.; Zhang, Y.; Li, P.; Gao, C. Strong, conductive, lightweight, neat graphene aerogel fibers with aligned pores. *ACS Nano* **2012**, *6*, 7103−7113.
(32) Hu, X.; Xu, Z.; Liu, Z.; Gao, C. Liquid crystal self-templating approach to ultrastrong and tough biomimic composites. *Sci. Rep.* **2013**, *3*, 2374.
(33) Liu, Z.; Xu, Z.; Hu, X.; Gao, C. Lyotropic liquid crystal of polyacrylonitrile-grafted graphene oxide and its assembled continuous strong nacre-mimetic fibers. *Macromolecules* **2013**, *46*, 6931−6941.
(34) Liu, J.; Chen, C.; He, C.; Zhao, L.; Yang, X.; Wang, H. Synthesis of graphene peroxide and its application in fabricating super extensible and highly resilient nanocomposite hydrogels. *ACS Nano* **2012**, *6*, 8194−8202.
(35) Liu, J.; Song, G.; He, C.; Wang, H. Self-healing in tough graphene oxide composite hydrogels. *Macromol. Rapid Commun.* **2013**, *34*, 1002−1007.
(36) Zhang, L.; Wang, Z.; Xu, C.; Li, Y.; Gao, J.; Wang, W.; Liu, Y. High strength graphene oxide/polyvinyl alcohol composite hydrogels. *J. Mater. Chem.* **2011**, *21*, 10399−10406.
(37) Fan, J.; Shi, Z.; Lian, M.; Li, H.; Yin, J. Mechanically strong graphene oxide/sodium alginate/polyacrylamide nanocomposite hydrogel with improved dye adsorption capacity. *J. Mater. Chem. A* **2013**, *1*, 7433−7443.
(38) Ma, X.; Li, Y.; Wang, W.; Ji, Q.; Xia, Y. Temperature-sensitive poly(*N*-isopropylacrylamide)/graphene oxide nanocomposite hydrogels by in situ polymerization with improved swelling capability and mechanical behavior. *Eur. Polym. J.* **2013**, *49*, 389−396.
(39) Shen, J.; Yan, B.; Li, T.; Long, Y.; Li, N.; Ye, M. Mechanical, thermal and swelling properties of poly(acrylic acid)−graphene oxide composite hydrogels. *Soft Matter* **2012**, *8*, 1831−1836.
(40) Song, G.; Zhang, L.; He, C.; Fang, D.-C.; Whitten, P. G.; Wang, H. Facile fabrication of tough hydrogels physically cross-linked by strong cooperative hydrogen bonding. *Macromolecules* **2013**, *46*, 7423−7435.
(41) Hontorialucas, C.; Lopezpeinado, A. J.; Lopezgonzalez, J. D. D.; Rojascervantes, M. L.; Martinaranda, R. M. Study of oxygen-containing groups in a series of graphite oxides—Physical and chemical characterization. *Carbon* **1995**, *33*, 1585−1592.
(42) Onsager, L. The effects of shape on the interaction of colloidal particles. *Ann. N. Y. Acad. Sci.* **1949**, *51*, 627−659.
(43) Donald, A. M. *Liquid Crystalline Polymers*, 2nd ed.; Cambridge University Press: Cambridge, England, 2006.
(44) Jalili, R.; Aboutalebi, S. H.; Esrafilzadeh, D.; Shepherd, R. L.; Chen, J.; Aminorroaya-Yamini, S.; Konstantinov, K.; Minett, A. I.; Razal, J. M.; Wallace, G. G. Scalable one-step wet-spinning of graphene fibers and yarns from liquid crystalline dispersions of graphene oxide: Towards multifunctional textiles. *Adv. Funct. Mater.* **2013**, *23*, 5345−5354.
(45) Kato, T.; Frechet, J. M. J. New approach to mesophase stabilization through hydrogen-bonding molecular-interactions in binary-mixtures. *J. Am. Chem. Soc.* **1989**, *111*, 8533−8534.
(46) Verhoeff, A. A.; Bakelaar, I. A.; Otten, R. H. J.; van der Schoot, P.; Lekkerkerker, H. N. W. Tactoids of plate-like particles: Size, shape, and director field. *Langmuir* **2011**, *27*, 116−125.
(47) Springer, G. H.; Higgins, D. A. Toroidal droplet formation in polymer-dispersed liquid crystal films. *J. Am. Chem. Soc.* **2000**, *122*, 6801−6802.
(48) Higgins, D. A.; Hall, J. E.; Xie, A. F. Optical microscopy studies of dynamics within individual polymer-dispersed liquid crystal droplets. *Acc. Chem. Res.* **2005**, *38*, 137−145.
(49) Lee, J. C. Polymerization-induced phase separation. *Phys. Rev. E* **1999**, *60*, 1930−1935.
(50) Serbutoviez, C.; Kloosterboer, J. G.; Boots, H. M. J.; Touwslager, F. J. Polymerization-induced phase separation. 2. Morphology of polymer-dispersed liquid crystal thin films. *Macromolecules* **1996**, *29*, 7690−7698.
(51) Wu, Z. L.; Arifuzzaman, M.; Kurokawa, T.; Furukawa, H.; Gong, J. P. Hydrogel with cubic-packed giant concentric domains of semi-rigid polyion complex. *Soft Matter* **2011**, *7*, 1884−1889.
(52) Wu, Z. L.; Kurokawa, T.; Liang, S.; Furukawa, H.; Gong, J. P. Hydrogels with cylindrically symmetric structure at macroscopic scale by self-assembly of semi-rigid polyion complex. *J. Am. Chem. Soc.* **2010**, *132*, 10064−10069.
(53) Wu, Z. L.; Kurokawa, T.; Liang, S.; Gong, J. P. Dual network formation in polyelectrolyte hydrogel via viscoelastic phase separation: Role of ionic strength and polymerization kinetics. *Macromolecules* **2010**, *43*, 8202−8208.
(54) Gong, J. P.; Katsuyama, Y.; Kurokawa, T.; Osada, Y. Double-network hydrogels with extremely high mechanical strength. *Adv. Mater.* **2003**, *15*, 1155−1158.
(55) Okumura, Y.; Ito, K. The polyrotaxane gel: A topological gel by figure-of-eight cross-links. *Adv. Mater.* **2001**, *13*, 485−487.
(56) Huang, T.; Xu, H.; Jiao, K.; Zhu, L.; Brown, H. R.; Wang, H. A novel hydrogel with high mechanical strength: A macromolecular microsphere composite hydrogel. *Adv. Mater.* **2007**, *19*, 1622−1626.
(57) Haraguchi, K.; Takehisa, T. Nanocomposite hydrogels: A unique organic−inorganic network structure with extraordinary mechanical, optical, and swelling/de-swelling properties. *Adv. Mater.* **2002**, *14*, 1120−1124.
(58) Nishida, T.; Obayashi, A.; Haraguchi, K.; Shibayama, M. Stress relaxation and hysteresis of nanocomposite gel investigated by SAXS and SANS measurement. *Polymer* **2012**, *53*, 4533−4538.